The Astrophysical Journal, 949:41 (9pp), 2023 June 1 https://doi.org/10.3847/1538-4357/acc86a
© 2023. The Author(s). Published by the American Astronomical Society.
OPEN ACCESS

The CGM^2 Survey: Quenching and the Transformation of the Circumgalactic Medium

Kirill Tchernyshyov[1], Jessica K. Werk[1], Matthew C. Wilde[1], J. Xavier Prochaska[2,3,4,12], Todd M. Tripp[5], Joseph N. Burchett[2,6], Rongmon Bordoloi[7], J. Christopher Howk[8], Nicolas Lehner[8], John M. O'Meara[9], Nicolas Tejos[10], and Jason Tumlinson[11]
[1] Department of Astronomy, University of Washington, Seattle, WA 98195, USA; ktcherny@gmail.com
[2] University of California, Santa Cruz, 1156 High Street, Santa Cruz, CA 95064, USA
[3] Kavli Institute for the Physics and Mathematics of the Universe (Kavli IPMU), The University of Tokyo, 5-1-5 Kashiwanoha, Kashiwa, 277-8583, Japan
[4] Division of Science, National Astronomical Observatory of Japan, 2-21-1 Osawa, Mitaka, Tokyo 181-8588, Japan
[5] Department of Astronomy, University of Massachusetts, 710 North Pleasant Street, Amherst, MA 01003-9305, USA
[6] Department of Astronomy, New Mexico State University, P.O. Box 30001, MSC 4500, Las Cruces, NM 88001, USA
[7] Department of Physics, North Carolina State University, Raleigh, NC 27695-8202, USA
[8] Department of Physics and Astronomy, University of Notre Dame, Notre Dame, IN 46556, USA
[9] W.M. Keck Observatory, 65-1120 Mamalahoa Highway, Kamuela, HI 96743, USA
[10] Instituto de Física, Pontificia Universidad Católica de Valparaíso, Casilla 4059, Valparaíso, Chile
[11] Space Telescope Science Institute, Baltimore, MD, USA
Received 2022 November 8; revised 2023 March 15; accepted 2023 March 27; published 2023 May 25

Abstract

This study addresses how the incidence rate of strong O VI absorbers in a galaxy's circumgalactic medium (CGM) depends on galaxy mass and, independently, on the amount of star formation in the galaxy. We use Hubble Space Telescope/Cosmic Origins Spectrograph absorption spectroscopy of quasars to measure O VI absorption within 400 projected kpc and 300 km s^{-1} of 52 galaxies with $M_* \sim 3 \times 10^{10}$ $M_\odot$. The galaxies have redshifts $0.12 < z < 0.6$, stellar masses $10^{10.1}$ $M_\odot < M_* < 10^{10.9}$ $M_\odot$, and spectroscopic classifications as star-forming or passive. We compare the incidence rates of high column density O VI absorption ($N_{\rm O\ VI} \geqslant 10^{14.3}$ cm^{-2}) near star-forming and passive galaxies in two narrow ranges of stellar mass and, separately, in a matched range of halo mass. In all three mass ranges, the O VI covering fraction within 150 kpc is higher around star-forming galaxies than around passive galaxies with greater than 3σ-equivalent statistical significance. On average, the CGM of star-forming galaxies with $M_* \sim 3 \times 10^{10}$ $M_\odot$ contains more O VI than the CGM of passive galaxies with the same mass. This difference is evidence for a CGM transformation that happens together with galaxy quenching and is not driven primarily by halo mass.

Unified Astronomy Thesaurus concepts: Circumgalactic medium (1879); Extragalactic astronomy (506); Quenched galaxies (2016)

1. Introduction

The circumgalactic medium (CGM) is the extended halo of gas surrounding a galaxy and a key site in the baryon cycle that governs a galaxy's supply of fuel for star formation. Its physical state mediates the accretion of intergalactic gas and can affect the outcome of feedback processes (i.e., whether winds stall or escape). The physical state of the CGM is set by the interaction of many factors: radiative cooling, the gravitational potential of the host dark matter halo, energy and momentum injection by feedback, and a variety of other possibly important influences such as cosmic rays and magnetic fields. Different relative contributions of these factors can yield qualitatively different CGM structures. A classic example is that when considering gravity and radiative cooling, maintaining a hot, quasi-static CGM inside a stable virial shock requires a sufficiently high halo mass (e.g., Birnboim & Dekel 2003; Dekel & Birnboim 2006). In the absence of other factors, intergalactic gas can accrete onto the host galaxies of lower-mass halos without shocking (e.g., White & Rees 1978; Kereš et al. 2005). How the balance of these factors affects and is affected by host galaxy properties is a key question for understanding galaxy evolution.

One part of this question is the role of the CGM in how central galaxies in subgroup-scale halos ($M_h \sim 10^{11}$–10^{12} $M_\odot$) quench. We are still learning how CGM observables differ around star-forming and passive galaxies. When comparing the CGM between these galaxy classes, it is necessary to control for a number of potentially confounding variables. CGM properties and observables depend on distance (observationally, on the impact parameter, $R_\perp$) from a galaxy, galaxy mass (stellar or halo) and color, redshift, environment, and, for some tracers, angular location relative to a galaxy (e.g., Bergeron 1986; Bahcall et al. 1991; Chen et al. 2001; Stocke et al. 2006; Bordoloi et al. 2011; Werk et al. 2013; Johnson et al. 2015; Burchett et al. 2016; Tejos et al. 2016). At the very least, it is necessary to control for impact parameter and galaxy mass and to restrict comparisons to reasonably narrow redshift ranges. Comparisons between star-forming and passive galaxies have been done with the necessary controls for cool ($T \sim 10^4$ K) metal-enriched gas traced by Mg II (Bordoloi et al. 2011; Lan 2020; Anand et al. 2021) and for hot ($T \gtrsim 10^6$ K) gas traced by X-ray emission (Chadayammuri et al. 2022; Comparat et al. 2022). Star-forming galaxies have higher equivalent widths of cool gas tracers than passive galaxies, but results are still unclear for X-ray emission.

[12] Simons Pivot Fellow.

Original content from this work may be used under the terms of the Creative Commons Attribution 4.0 licence. Any further distribution of this work must maintain attribution to the author(s) and the title of the work, journal citation and DOI.

There is a paucity of constraints on gas in the intermediate temperature range, $T \sim 10^5$ K. When metal-enriched, gas in this temperature range can be traced by the ion O VI. This gas may be near thermal equilibrium (Voit 2019; Faerman et al. 2020) or it may be part of cooling inflows or outflows (Heckman et al. 2002; Bordoloi et al. 2017; McQuinn & Werk 2018; Qu & Bregman 2018). Some O VI may instead be tracing cool gas ($T \sim 10^4$ K) that is diffuse enough for the extragalactic background to photoionize oxygen to O VI ($n_{\rm H} \sim 10^{-5}$–10^{-4} cm^{-3}, Tripp et al. 2008; Stern et al. 2018). Ne VIII measurements strongly suggest the presence of a warm–hot phase (Burchett et al. 2018).

Low-redshift star-forming galaxies in general (i.e., without controlling for galaxy mass) have higher detection rates and typical O VI column densities than passive galaxies (Tumlinson et al. 2011; Johnson et al. 2015; Zahedy et al. 2019). The only mass-controlled comparison of O VI absorber statistics between star-forming and passive galaxies thus far is found in the supplementary materials of Tumlinson et al. (2011), but its results are inconclusive. Because the star-forming galaxies in all other comparisons have lower average masses than the passive galaxies, the interpretation of the difference in O VI absorber statistics is ambiguous: is the O VI dichotomy driven by differences in halo mass or is it the result of some distinct process associated with quenching?

Which interpretation is correct bears on the connection between feedback, the CGM, and galaxy quenching. If there is no difference in O VI around star-forming and passive galaxies at fixed mass, then the O VI dichotomy is caused by a change in CGM structure as a function of halo mass and the different halo mass distributions of star-forming and passive galaxies. This scenario has been suggested in works such as Oppenheimer et al. (2016), Fielding et al. (2017), and Sanchez et al. (2019). If instead there is a difference at fixed mass, then the O VI dichotomy is caused by some process other than the quasi-hydrostatic evolution of a growing halo. The clearest prediction from a simulation for a difference in O VI column density at fixed mass is found in Nelson et al. (2018). In that work and similar ones, the mechanism responsible is integrated feedback from an active galactic nucleus that heats and partially drives out the CGM (Mathews & Prochaska 2017; Suresh et al. 2017; Davies et al. 2020; Oppenheimer et al. 2020; Terrazas et al. 2020; Zinger et al. 2020). Finding that the O VI dichotomy persists at fixed mass would not automatically mean that quenching disrupts the CGM or that some change in the CGM causes quenching: both changes could be caused by a third process, such as interaction with large-scale structure. However, it would mean a more direct connection between the state of a galaxy and its CGM than the scenario where star-forming and passive galaxies of the same mass can have the same CGM.

In this work, we compare O VI incidence rates around star-forming and passive galaxies with stellar masses (M_*) between $10^{10.1}$ and $10^{10.9}$ $M_\odot$, controlling for impact parameter and stellar mass and, in a separate comparison, approximately controlling for halo mass (M_h). For the halo mass comparison, we account for the different clustering properties of star-forming and passive galaxies by using star formation-dependent stellar-mass-to-halo-mass relations when estimating halo masses. We build our sample by combining galaxy–O VI absorber pairs from a compilation of new and literature measurements published in Tchernyshyov et al. (2022, Paper I) with a small number of additional observations from the CUBS survey (Chen et al. 2020). The data set is described in Section 2. The mass-controlled comparison between star-forming and passive galaxies is described in Section 3. We discuss the implications of our findings in Section 4 and summarize our results in Section 5. We assume a flat-universe ΛCDM cosmology with $H_0 = 67.8$ km s^{-1} Mpc^{-1} and $\Omega_m = 0.308$ (Planck Collaboration et al. 2016). Stellar masses are derived assuming a Chabrier (2003) initial mass function.

2. Data

We analyze a set of galaxy–O VI absorber pairs matched in mass and impact parameter. Most of the galaxy masses, impact parameters, and associated O VI column densities are taken from the galaxy–absorber data compiled in Paper I. This data set combines measurements from the CGM^2 survey (Wilde et al. 2021) and the literature (Werk et al. 2013; Johnson et al. 2015; Keeney et al. 2018; Zahedy et al. 2019). We also include three galaxy–absorber pairs from the CUBS survey (Chen et al. 2020; Boettcher et al. 2021; Cooper et al. 2021; Zahedy et al. 2021). In cases where information on galaxy environment is available, we exclude galaxies from our analysis if they are within 1 Mpc and 600 km s^{-1} of a more massive galaxy. In Paper I, O VI absorbers are associated with a galaxy if they are within ±300 km s^{-1} of the galaxy's redshift. We keep this convention in this work.

We do not use the galaxy classifications from Paper I, which were based on fitting galaxy templates to photometric measurements. Instead, we use spectroscopic classifications. For galaxies from Johnson et al. (2015) and the CUBS survey, we adopt the classifications given in those works. For the remainder of the sample, we make our own spectroscopic classifications.

We use three classification criteria: equivalent width of Hα emission, equivalent width of Hβ emission, and the 4000 Å decrement D_{4000}.[13] We use multiple criteria because the galaxy spectra were taken with different instruments and cover different ranges of galaxy rest-frame wavelength. We measure Hα and Hβ equivalent widths by fitting the galaxy spectra with superpositions of stellar templates and emission lines. Fitting is done with `pPXF` (Cappellari 2017) using the MILES stellar library (Falcón-Barroso et al. 2011). We measure D_{4000} by integrating the galaxy spectra over the appropriate interval and taking the ratio of the results.

Not all quantities are measurable from all spectra. Of the ones that are measured from a spectrum, we adopt the classification according to the *most preferred* quantity, where the order of preference is Hα, then Hβ, then D_{4000}. A galaxy is classified as star-forming if it has an Hα equivalent width greater than 6 Å, an Hβ equivalent width greater than 2 Å, or D_{4000} less than 1.6 (Kauffmann et al. 2003; Sánchez et al. 2014). The quantities usually agree on a galaxy's classification. Taken pairwise, Hα and Hβ, Hα and D_{4000}, and Hβ and D_{4000} agree in 42/42, 34/36, and 41/49 instances, respectively.

The cuts on star formation indicators split the galaxies at low impact parameters into mostly low and mostly high $N_{\rm O\,VI}$ subsamples. Figure 1 shows $N_{\rm O\,VI}$ as a function of the three indicators around galaxies with $R_\perp < 200$ kpc. The two star-forming $N_{\rm O\,VI}$ nondetections have larger impact parameters

[13] We use the 100 Å wide interval definition of D_{4000}, with intervals 3850–3950 and 4000–4100 Å (Balogh et al. 1999).

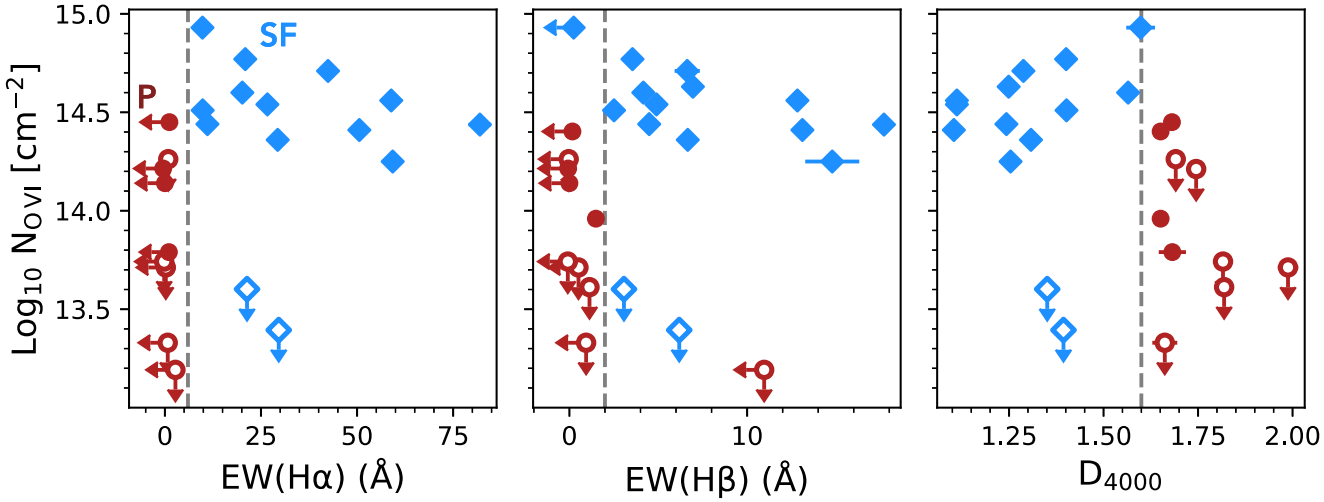

Figure 1. O VI column density as a function of three star formation indicators for galaxies with $R_\perp < 200$ kpc. Data point colors and shapes denote whether a galaxy is classified as star-forming (blue diamonds) or passive (red and red-outlined circles). Data points with a blue or red outline and white interior are upper limits on O VI nondetections. Because not all galaxies have measurements of all three indicators, some points only appear in some of the panels. Vertical dashed gray lines denote thresholds used for galaxy classification and were taken from the literature. The three star formation indicators almost always agree on a galaxy's class. There is a clear change in the $N_{\rm O\ VI}$ distribution from one side of a classification threshold to the other.

than all but one of the other star-forming galaxies shown. Apart from these two nondetections, galaxies on the star-forming side of the classification thresholds have higher $N_{\rm O\ VI}$ than most passive galaxies.

Galaxies where the star formation indicators are not unanimous have column densities that are consistent with their assigned class. There are nine such galaxies: five classified as star-forming and four classified as passive. All four of the passive galaxies have $N_{\rm O\ VI}$ nondetections. Two of the star-forming galaxies are about 40 kpc from the sight line and have detected $N_{\rm O\ VI}$ values that are similar to those of other low-$R_\perp$ star-forming galaxies. The remaining three have $R_\perp > 170$ kpc and have $N_{\rm O\ VI}$ nondetections, which is typical of high-$R_\perp$ star-forming galaxies in the sample.

We focus on galaxies with stellar masses between $10^{10.1}$ and $10^{10.9}$ $M_\odot$. Paper I included galaxies with masses ranging from $10^{7.8}$ to $10^{11.2}$ $M_\odot$. In that sample, the overwhelming majority of photometrically classified passive galaxies have $M_* \geqslant 10^{10}$ $M_\odot$. For this work, we initially spectroscopically classified all of those galaxies with $M_* \geqslant 10^{10}$ $M_\odot$. The sample contains no passive galaxies with mass less than $10^{10.1}$ $M_\odot$ and no star-forming galaxies with mass greater than $10^{10.9}$ $M_\odot$. To get a closer match in M_*, we restrict the sample to bracket this mass range. The stellar masses and impact parameters of galaxies in this range are shown in Figure 2.

To enable a test of the hypothesis that differences between star-forming and passive galaxies are driven by halo mass, we estimate halo masses for the galaxies in the sample. We match the observed galaxies to central galaxies from the UNIVERSEMACHINE mock catalogs (Behroozi et al. 2019), conditioning on star formation class, stellar mass, and redshift. We classify mock galaxies to be star-forming or passive using a specific star formation (sSFR) cut of 10^{-11} yr^{-1}, use a tolerance of ± 0.01 dex for matching on stellar mass, and take the nearest redshift available (in all cases, $|\delta z| \leqslant 0.1$). This procedure yields between 800 and 2800 matching mock galaxies per observed galaxy, each with a halo mass. We summarize an observed galaxy's possible halo mass distribution by its 16th, 50th, and 84th percentiles. The median halo

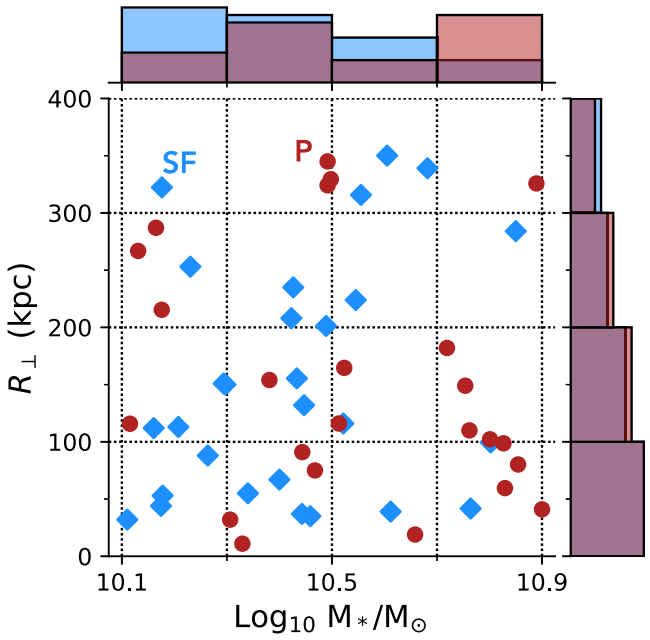

Figure 2. Stellar masses and impact parameters of galaxies in the sample. Blue diamonds represent star-forming galaxies, red circles represent passive galaxies. The distribution of the two classes in stellar mass is shown by the histogram above the scatter plot.

masses of the star-forming and passive samples overlap for $M_h \approx 10^{11.6}$–$10^{12.2}$ $M_\odot$. With this procedure for estimating halo mass, star-forming and passive galaxies in this halo mass range have $M_* = 10^{10.2}$–$10^{10.9}$ $M_\odot$ and $M_* = 10^{10.1}$–$10^{10.7}$ $M_\odot$, respectively.

We compare star-forming and passive galaxies in three mass subsamples: $M_* = 10^{10.1}$–$10^{10.5}$ $M_\odot$ (lower stellar mass), $M_* = 10^{10.5}$–$10^{10.9}$ $M_\odot$ (higher stellar mass), and $M_h \approx 10^{11.6}$–$10^{12.2}$ $M_\odot$ (matched halo mass). The matched halo mass subsample partially overlaps with each of the matched stellar mass subsamples. The impact parameters and O VI column densities of galaxies in these subsamples are shown in Figure 3. The right panel shows a subset of the

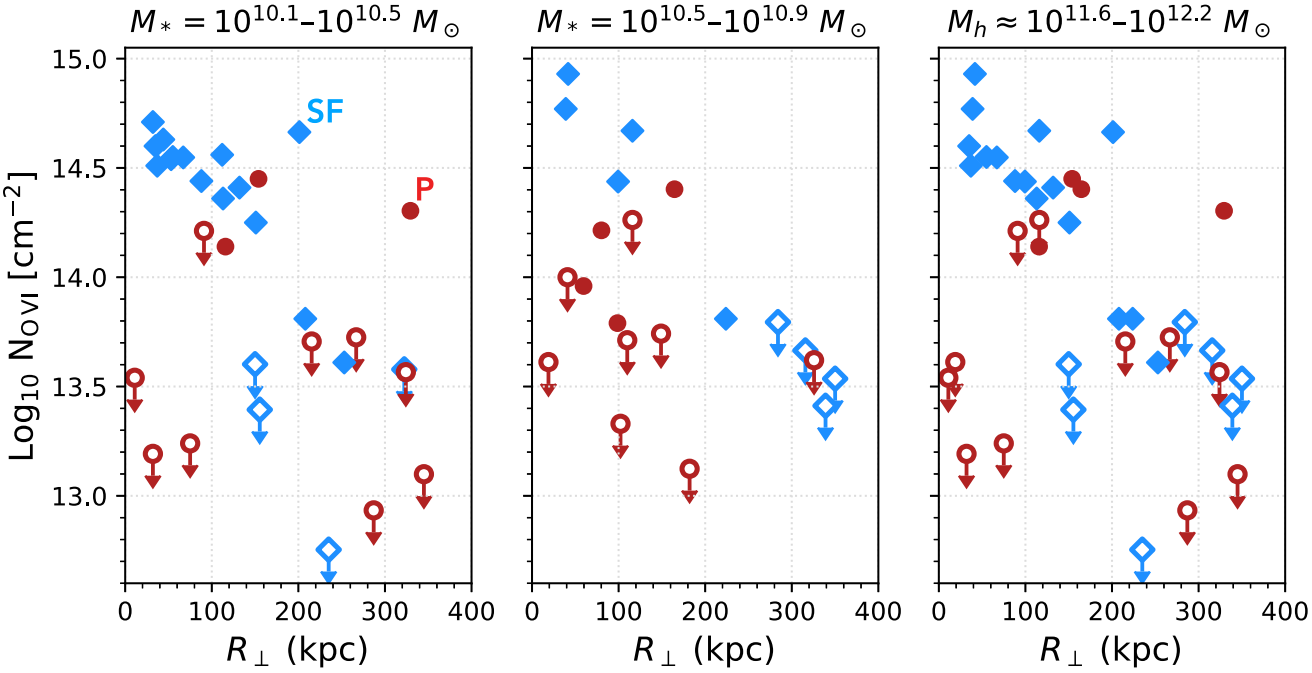

Figure 3. O VI column density as a function of impact parameter for three mass-selected comparison samples of star-forming and passive galaxies. Filled data points mark O VI detections while outlined data points with a white interior mark upper limits on nondetections. Blue diamonds are star-forming galaxies and red circles are passive galaxies. The left and middle panels show galaxies selected to be in the same stellar mass range. The right panel shows galaxies selected to be in the same halo mass range, where halo masses are estimated using separate stellar mass–halo mass relations for the two galaxy classes. The halo mass-selected sample overlaps with both stellar mass-selected samples.

galaxies in the left and middle panels. The distributions of measurements in all three panels are qualitatively similar. Star-forming galaxies have distinct inner and outer column density regimes, with uniformly high column densities in the inner region and a broad, generally lower distribution of column densities in the outer region. Passive galaxies have a broad distribution of column densities at all impact parameters. The inner column densities of star-forming galaxies are greater than almost all of those of passive galaxies.

3. Analysis and Results

We quantify the incidence of strong O VI absorbers around star-forming and passive galaxies by calculating covering fractions, the number of detections above a threshold ("hits") over the number of observations. We adopt a detection threshold of $N_{\mathrm{O\,VI}} = 10^{14.3}$ cm^{-2}, which is just above the least constraining upper limit in the sample. An upper limit that is greater than the threshold is ambiguous, meaning that using a lower threshold would require discarding part of the sample.

The number of hits in a sample of fixed size given a covering fraction has a binomial distribution. Assuming a beta distribution prior on the covering fraction, the posterior probability distribution for the covering fraction is itself a beta distribution. We use the Jeffreys prior, Beta(f_C; $\alpha = 1/2$, $\beta = 1/2$), and use the 16th and 84th quantiles of the posterior probability distribution over the covering fraction as a 68% (1σ-equivalent) credible interval.

From visual inspection of Figure 3, there is an obvious need for covering fractions to depend on impact parameter. We include an impact parameter dependence by splitting each mass-selected subsample into inner and outer regions. Figure 4 shows inner and outer covering fractions for the three mass subsamples and a dividing $R_\perp$ of 200 kpc. The inner covering fraction around star-forming galaxies is higher than that around passive galaxies. The outer covering fractions of the two galaxy classes are consistent, with overlapping 68% credible intervals.

To quantitatively compare the inner covering fractions for the two galaxy classes, we calculate their ratio as a function of maximum inner impact parameter. The top row of Figure 5 shows inner covering fractions at all impact parameters spanned by each mass-selected subsample. These covering fractions are cumulative: measurements used to calculate the covering fraction at $R_{\perp,1}$ are also used to calculate the covering fraction at $R_{\perp,2} > R_{\perp,1}$. The covering fractions of O VI absorbers around star-forming galaxies decline outside about 150 kpc. Those of O VI absorbers around passive galaxies are similar at all impact parameters. The middle row shows the ratio $f_{C,\mathrm{P}}/f_{C,\mathrm{SF}}$. The probability distribution over the ratio is estimated by integrating over the joint distribution of the two covering fractions, $p(f_{C,\mathrm{P}}, f_{C,\mathrm{SF}})$, over lines of fixed ratio.

The bottom row of the figure shows the probability that this ratio is greater than one. We consider a probability less than about 0.00135 to be statistically significant evidence[14] that $f_{C,\mathrm{SF}}$ is greater than $f_{C,\mathrm{P}}$. If there are too few measurements, the probability will be above this threshold even for the most favorable set of measurements. For example, a sample of seven star-forming and two passive galaxies can never give a statistically significant result, not even if all the star-forming galaxies are detections and all the passive galaxies are nondetections. Ranges of impact parameter where there are too few measurements are indicated in the bottom row of Figure 5 by gray rectangles.

[14] This is the probability of drawing a value that is lower than $\mu - 3\sigma$ from a Gaussian distribution.

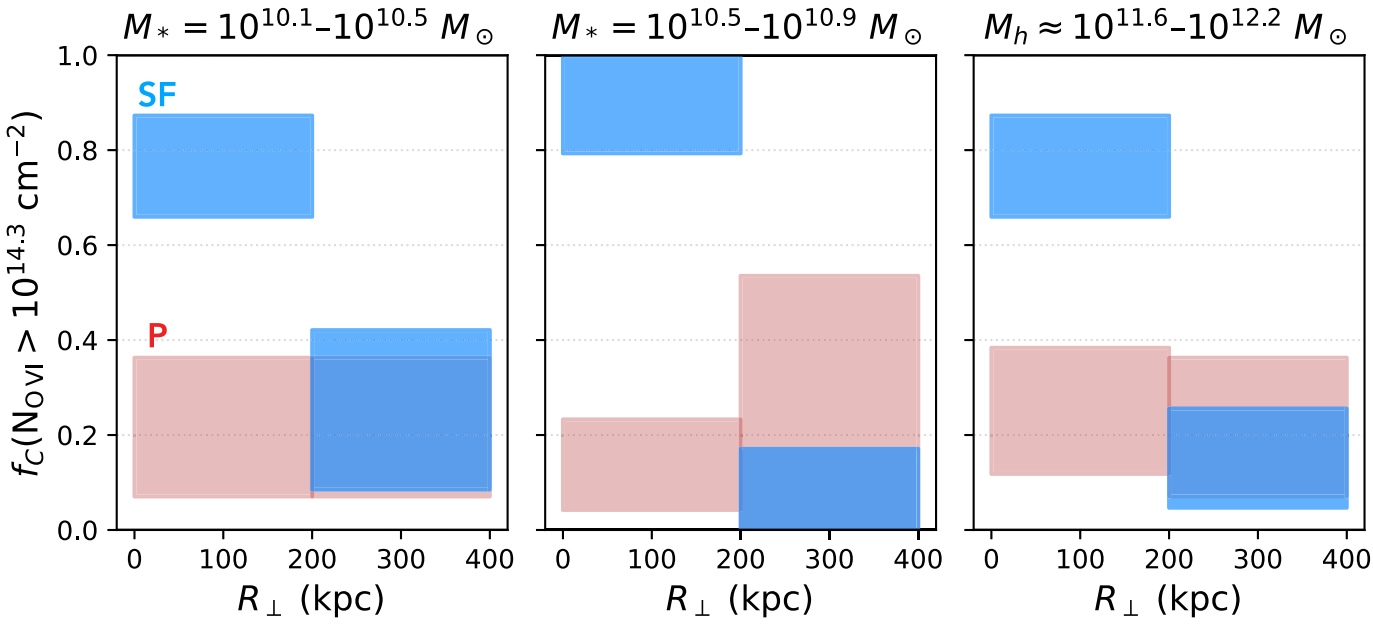

Figure 4. O VI covering fractions around star-forming (blue) and passive (red) galaxies in three mass-selected samples. Shaded regions are 68% credible intervals about the median for the covering fraction of absorbers with $R_\perp = 0$–200 kpc and 200–400 kpc. Star-forming galaxies have higher inner covering fractions than passive galaxies, but similar outer covering fractions.

For all maximum impact parameters that are less than about 150 kpc and where there are enough measurements, the probability is below the threshold. The decrease in significance for greater dividing impact parameters is likely physical and can be explained by the decline in the covering fraction of O VI absorbers around star-forming galaxies. In all three mass-matched subsamples, there are significantly more strong O VI absorbers near star-forming galaxies than near passive galaxies. These results show that there is a statistically significant dichotomy in O VI around star-forming and passive galaxies at fixed stellar mass and at fixed halo mass.

4. Discussion

4.1. Comparison with Previous Work on O VI and Star Formation

The present study builds on Tumlinson et al. (2011), which found that there is a higher incidence rate of strong O VI absorption around star-forming galaxies than around passive galaxies at $0.1 < z < 0.4$. The supplementary material of Tumlinson et al. (2011) contains a comparison of O VI detection rates between the galaxy classes restricted to a mass range where star-forming and passive galaxies in their sample overlap, $M_* > 10^{10.5}\ M_\odot$. They find that with 2.6σ-level significance, the detection rate is higher for star-forming galaxies, a suggestive result that motivated our current work.

Like a number of other observational studies (Johnson et al. 2015; Zahedy et al. 2019), we confirm the general finding that there is an O VI dichotomy between star-forming and passive galaxies. We extend the result by establishing with high statistical significance that the dichotomy persists when controlling for stellar mass or halo mass. The difference in O VI incidence around passive galaxies is evidence for a CGM transformation that is associated with how central galaxies in this mass range quench.

4.2. Galaxy Quenching and CGM Transformation

Recent theory and analyses of cosmological hydrodynamic simulations offer a candidate for the required CGM transformation: the heating and ejection of CGM gas by integrated black hole feedback (Mathews & Prochaska 2017; Suresh et al. 2017; Davies et al. 2020; Oppenheimer et al. 2020; Terrazas et al. 2020; Zinger et al. 2020). In the EAGLE and IllustrisTNG simulations, galaxies quench when the integrated amount of black hole feedback exceeds the binding energy of the CGM and ejects some fraction of it from the halo. The bulk of the gas remaining in the CGM after quenching is hotter and more diffuse than before, and as a result has a long cooling time. Nelson et al. (2018) find that in IllustrisTNG, the O VI mass also drops once a galaxy quenches. This galaxy quenching mechanism is consistent with our observations (and some observational studies of central galaxy quenching, e.g., Reines & Volonteri 2015; Piotrowska et al. 2022) because its onset is determined by black hole mass rather than by galaxy stellar mass or halo mass. Other quenching mechanisms, such as those in which the interaction of a halo with large-scale structure cuts off the supply of intergalactic gas to the central galaxy (Aragon Calvo et al. 2019; Winkel et al. 2021), would also be consistent.

4.2.1. High Passive Galaxy $N_{O\,VI}$: Geometric, Temporal, or Mechanical Variation?

While most absorbers associated with passive galaxies have low O VI column densities, this is not universal. Of the 16 passive galaxies in our sample with $R_\perp < 200$ kpc, two have $N_{O\,VI}$ values typical of star-forming galaxies. Put another way, the distribution $p(N_{O\,VI})$ for sight lines near passive galaxies is shifted to lower $N_{O\,VI}$ compared to $p(N_{O\,VI})$ for star-forming galaxies, but does have a high $N_{O\,VI}$ tail.

The simplest explanations for these two cases are misclassification or interloping absorption. Both galaxies have secure classifications, with very low equivalent widths of

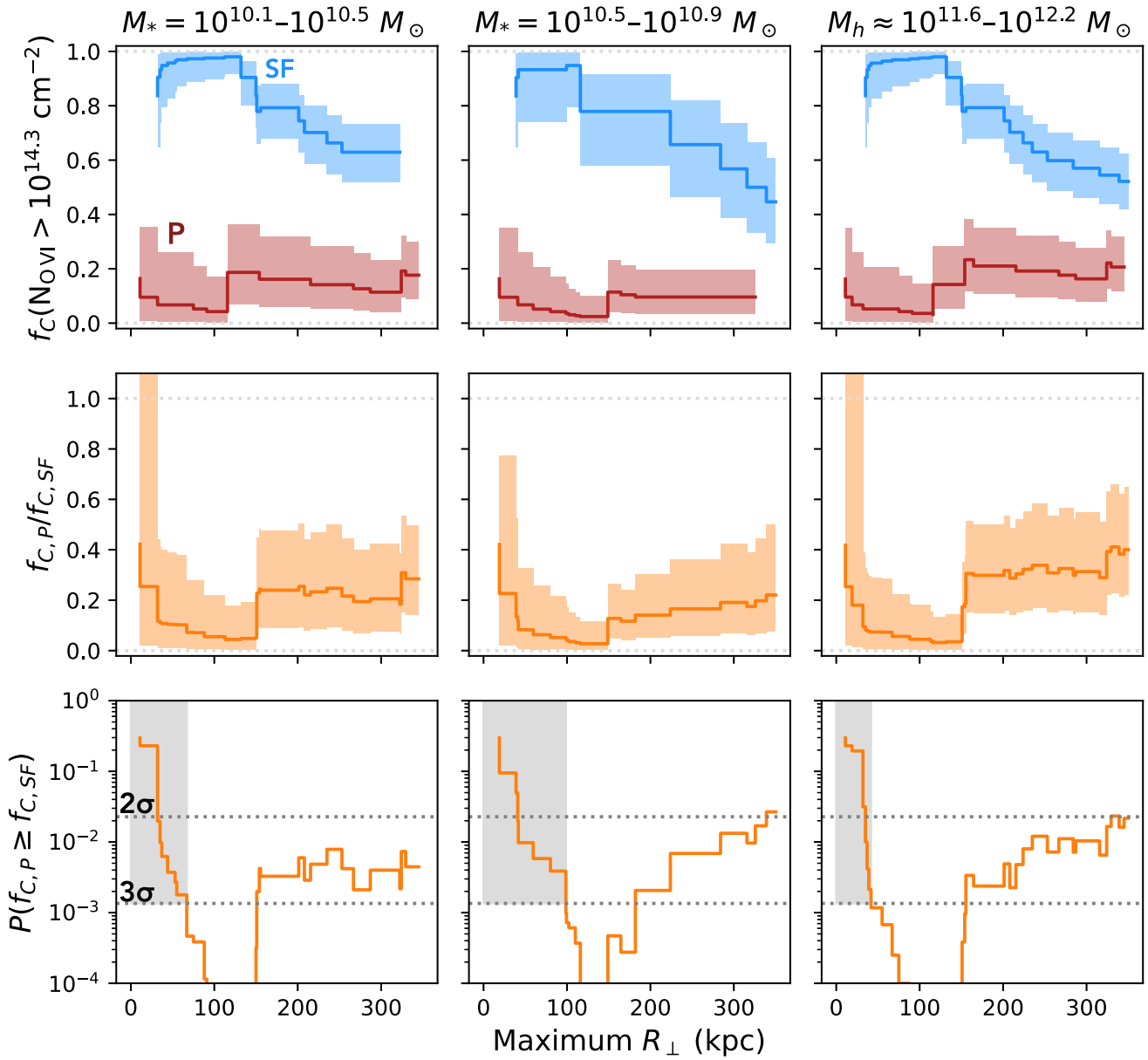

Figure 5. Top row: O VI covering fractions within a maximum impact parameter of star-forming (blue) and passive (red) galaxies in three mass-selected samples. In this row and the next, solid lines are medians and shaded regions are central 68% credible intervals. Middle row: ratio of the covering fraction of O VI absorbers around passive galaxies to the covering fraction of O VI absorbers around star-forming galaxies. Bottom row: probability that the covering fraction of O VI absorbers around passive galaxies is greater than or equal to that of O VI absorbers around star-forming galaxies. One-sided 2σ- and 3σ-equivalent probabilities are indicated by horizontal lines. Maximum impact parameters where the probability can never be less than 3σ-equivalent because there are too few measurements are shaded in gray. The covering fraction of O VI absorbers around star-forming galaxies declines for maximum impact parameters greater than approximately 150 kpc. Between the region with too few measurements and 150 kpc, the covering fraction of O VI absorbers around star-forming galaxies is greater than that of O VI absorbers around passive galaxies with conclusive, greater than 3σ-equivalent statistical significance.

hydrogen emission and D_{4000} values that are greater than the threshold of 1.6. Their D_{4000} values are less than the median for the passive galaxy sample, so there is a possibility that these galaxies quenched relatively recently.

Interloping absorption can be significant: Ho et al. (2021) find that in the EAGLE simulations, the column density of O VI absorbers within ± 300 km s^{-1} of a galaxy can be twice that of absorbers with radius less than $R_{\rm vir}$. This could be the explanation for one of the galaxies, where we do not have good information on environment. The other galaxy is found in a CGM^2 quasar field with spectroscopy that is complete to a g-band magnitude of 22 within 600 kpc, a depth sufficient to detect galaxies down to $M_* \sim 10^{9.5}\ M_\odot$. No other galaxies are detected within 600 kpc of the sight line and 600 km s^{-1} of the passive galaxy in question, suggesting that the high O VI column density is not attributable to an interloping galaxy's CGM.

Possible physical explanations for the the high $N_{\rm O\,VI}$ tail include a patchy O VI distribution, a lag between quenching and CGM transformation, and a secondary channel for quenching without a CGM transformation. If O VI around a typical passive galaxy is found in localized, anisotropically distributed structures, the low sample-averaged O VI incidence rate would reflect a low per-galaxy O VI covering fraction.

However, these structures would need to have total O VI column densities close to those of sight lines through a star-forming galaxy's CGM. A different explanation is that the CGM transformation as seen in O VI starts later or takes longer than quenching. In this interpretation, the passive galaxies with high $N_{\rm O\,VI}$ column densities are ones that quenched recently. Finally, there may be galaxies whose sSFR is low because of effects internal to the galaxy. Structures such as bars can reduce the star formation efficiency of gas in a galaxy without affecting the CGM (e.g., "morphological quenching" or "bar quenching"; Tubbs 1982; Martig et al. 2009; Khoperskov et al. 2018; Newnham et al. 2020).

Examples of the first two options, O VI patchiness in passive galaxy halos and a lag between quenching and CGM transformation, have been seen in cosmological hydrodynamic simulations. Nelson et al. (2018) find that in the TNG100 simulation, the O VI distribution is smooth and approximately isotropic around star-forming galaxies but patchy and lopsided around passive galaxies. Oppenheimer et al. (2020) analyze the coevolution of black hole mass, star formation rate, and the CGM in the EAGLE simulation and find that covering fractions of CGM ion absorption decline about 1 Gyr after quenching. Appleby et al. (2023) find that "green valley" galaxies in the SIMBA simulation have covering fractions of strong O VI absorbers that are lower than those of star-forming galaxies but higher than those of passive galaxies. Our two-category scheme would classify their green valley galaxies as also being passive, making this another example of a delay between quenching and CGM transformation.

While all three of these simulations show a decline in the incidence rate of O VI absorption as a result of integrated black hole feedback, they implement the feedback in different ways (Schaye et al. 2015; Weinberger et al. 2017; Davé et al. 2019). The feedback schemes lead to different values for bulk CGM properties such as CGM mass as a fraction of halo mass (e.g., Davies et al. 2021; Tillman et al. 2023). It is therefore plausible that while black hole feedback is involved in all three cases, the actual mechanisms by which O VI incidence is suppressed are not the same.

Conversely, a common (if not dominant) mechanism for quenching central galaxies without a CGM transformation is not seen in recent cosmological hydrodynamic simulations. A mechanism of this sort, bar quenching, is one of the proposed explanations for passive disk galaxies ("red spirals"; Masters et al. 2010). Studies of central red spirals in the EAGLE and IllustrisTNG simulations conclude that they are quenched in the same way as other passive centrals: through gas expulsion by black hole feedback (Correa et al. 2019; Davies et al. 2020; Łokas 2022; Park et al. 2022). At least in IllustrisTNG, red spirals tend to have quenched more recently than red ellipticals. A difference in CGM properties between red spirals and red ellipticals could therefore be an indication of a delay in the observability of the CGM transformation. Curiously, one of the two high-$N_{\rm O\,VI}$ passive galaxies introduced at the beginning of this subsection appears to be an edge-on disk; the morphology of the other galaxy is unclear from the limited imaging data that are available.

4.2.2. The Case of M31

The Milky Way's nearest massive neighbor, M31, can be used as a case study for elevated O VI around a passive galaxy. M31 has a stellar mass of $10^{10.93}$ $M_\odot$ and a specific star formation rate of $7\times10^{-12}\,{\rm yr}^{-1}$ (Lewis et al. 2015; Williams et al. 2017). By the definitions of our sample, M31 is passive and just barely more massive than the upper end of our higher stellar mass bin. The black hole mass of M31 is $(1.1–2.3)\times10^8$ $M_\odot$ (Bender et al. 2005), which is at or above the black hole mass associated with quenching in the IllustrisTNG and EAGLE simulations (Oppenheimer et al. 2020; Terrazas et al. 2020). Despite being passive, M31 has a disk and an H I mass of 5×10^9 $M_\odot$ (Carignan et al. 2006). Its $M_{\rm H\,I}/M_*$ is about 0.06, average for a $z<0.05$ galaxy of its stellar mass (Catinella et al. 2012).

M31's CGM has been measured using UV absorption spectroscopy along 43 quasar sight lines going out to $R_\perp=569$ kpc (Lehner et al. 2015, 2020). Eight of the sight lines within $R_\perp<400$ kpc include measurements of O VI, and seven of these eight have $N_{\rm O\,VI}\geqslant10^{14.3}$ cm^{-2}. This high covering fraction out to 400 kpc is inconsistent with what we see for both passive and star-forming galaxies. In the high-M_* subsample of passive galaxies, the corresponding hit rate is one out of 12. Using Barnard's exact test for 2-by-2 contingency tables (Barnard 1947), the probability of M31 having a covering fraction that is less than or equal to that of the passive subsample is less than 0.1%, a greater-than-3σ tension. The tension with the star-forming galaxy sample is at high $R_\perp$: all of the $N_{\rm O\,VI}$ measurements in M31 at $R_\perp>200$ kpc are greater than all of the corresponding $N_{\rm O\,VI}$ measurements in the high-M_* star-forming subsample.

These two inconsistencies may have different causes. The large extent relative to star-forming galaxies may be due to the presence of nonaxisymmetric structure near M31. Qu et al. (2021) find evidence for a massive bridge containing hot, $\sim10^6$ K gas between the Milky Way and M31, and similar structures are found in simulations of Local Group analogues (Nuza et al. 2014; Damle et al. 2022). The extended O VI could arise in cooler gas within this same bridge. Lehner et al. (2020) suggest that the distant O VI is associated with an accreting filament of the intergalactic medium. In either case, the structure would have a high covering fraction when viewed along a spatially clustered set of sight lines from the correct vantage point but could have a much lower covering fraction in a set of single–sight line measurements taken from random vantage points.

The high O VI covering fraction relative to our passive sample could be explained by temporal variation or by a form of quenching that does not involve the CGM. M31's star formation rate was several times higher 100 Myr ago (Lewis et al. 2015) and substantially higher 1–2 Gyr ago (Williams et al. 2017). M31 became passive at some point in this time range, with the exact "time of quenching" depending on one's choice of an sSFR threshold between passive and star-forming galaxies. A delay of 0.1–1 Gyr between quenching and a detectable change in the CGM is reasonable. M31 is also known to have a bar, and so could be passive due to internal dynamical effects that are irrelevant for its CGM (Athanassoula & Beaton 2006; Dorman et al. 2015; Feng et al. 2022).

4.3. Cool and Hot Gas in the CGM of Quenched Galaxies

If O VI around galaxies with $M_*=10^{10}$–10^{11} $M_\odot$ is mostly collisionally ionized and found in $\sim10^5$ K gas, then the O VI dichotomy implies that quenching is associated with a drop in the amount of warm gas in a galaxy's CGM. There is evidence that passive galaxies in the same mass range also have less $T\sim10^4$ K gas than the corresponding star-forming galaxies.

Cool gas is traced by ions such as Mg II. Analyses of the covering fractions of strong Mg II absorbers as a function of impact parameter, stellar mass, and star formation rate find that the covering fraction is several times lower near passive galaxies than near star-forming galaxies (Bordoloi et al. 2011; Lan 2020; Anand et al. 2021).

The situation is less clear for gas that is too hot to be traced by O VI ($T \gtrsim 10^6$ K). Emission from hot gas can be detected in X-rays. Comparat et al. (2022) and Chadayammuri et al. (2022) use eROSITA data to measure X-ray emission around stellar-mass-controlled samples of star-forming and passive galaxies and find conflicting results. Comparat et al. (2022) find that passive galaxies are associated with more X-ray emission while Chadayammuri et al. (2022) find the opposite. Chadayammuri et al. (2022) argue that the discrepancy is driven by differences in how emission from groups and clusters is treated for galaxies other than the group and cluster centrals. Determining which interpretation of the data is correct will tell us whether the CGM transformation associated with quenching mostly heats gas or also drives some of it out of the halo. If warm gas is driven out as well as heated, the X-ray emission from passive galaxies should be weaker. If the gas is heated but remains in the CGM, then the X-ray emission from passive galaxies should be stronger.

5. Conclusion

We study the incidence rate of strong O VI absorption in the CGM of $z < 0.6$ star-forming and passive central galaxies with stellar masses between $10^{10.1}$ and $10^{10.9}$ $M_\odot$. The sample of galaxy–O VI absorber pairs is drawn from Tchernyshyov et al. (2022) and references therein and from the CUBS survey (Chen et al. 2020). The absorber impact parameters span ≈0–400 physical kpc. To separate differences due to galaxy stellar or halo mass from differences related to galaxy quenching, we compare the two galaxy classes in narrow stellar mass ranges, $M_* = 10^{10.1}$–$10^{10.5}$ $M_\odot$ and $M_* = 10^{10.5}$–$10^{10.9}$ $M_\odot$, and, separately, in a relatively narrow range of estimated halo mass, $M_h \approx 10^{11.6}$–$10^{12.2}$ $M_\odot$.

For each combination of mass range and galaxy class, we further split the galaxies by impact parameter into inner and outer regions. We measure covering fractions of sight lines with $N_{\rm O\,VI} \geqslant 10^{14.3}$ cm^{-2} for these two regions and calculate probabilities that the inner covering fractions of O VI absorbers around star-forming galaxies are less than or equal to those around passive galaxies. We also explore some possible origin scenarios for the small number of strong O VI absorbers that are still found around passive galaxies.

Our observational results on the incidence rate of strong O VI absorbers around star-forming and passive galaxies in the mass ranges $M_* = 10^{10.1}$–$10^{10.5}$ $M_\odot$, $M_* = 10^{10.5}$–$10^{10.9}$ $M_\odot$, and $M_h \approx 10^{11.6}$–$10^{12.2}$ $M_\odot$ are as follows:

1. Within 150 kpc, the covering fraction of strong O VI absorbers is approximately 0.9–1 for star-forming galaxies and 0–0.2 for passive galaxies.
2. In each mass range and within 150 kpc, the probability that covering fractions of O VI absorbers around star-forming galaxies are less than or equal to those around passive galaxies is less than 0.001. At greater than 3σ-equivalent statistical significance, the incidence rate of strong O VI absorption in the CGM is greater around star-forming galaxies than around passive galaxies with the same stellar or halo mass.

From these observational results, we reach the following conclusions:

1. There is a dichotomy in the incidence rate of strong O VI absorption in the CGM of star-forming and passive galaxies with $M_* \sim 3 \times 10^{10}$ $M_\odot$ at fixed stellar mass and at fixed halo mass.
2. The quenching of a central galaxy with $M_* \sim 3 \times 10^{10}$ $M_\odot$ at low redshift is, in most cases, accompanied by a transformation of the galaxy's CGM. This change is not driven by the mass of the galaxy's dark matter halo.
3. There may be a delay between galaxy quenching and an observable change in the incidence rate of O VI. Alternatively (or jointly), there may be a less common mode of quenching in which the CGM is not substantially changed.

K.T. thanks Alison Coil, Yakov Faerman, Chris McKee, Evan Schneider, Fakhri Zahedy, and Yong Zheng for useful discussions and the referee for a helpful and constructive report. K.T., J.K.W., and M.W. acknowledge support for this work from NSF-AST 1812521 and NSF-CAREER 2044303. J. K.W. acknowledges additional support as a Cottrell Scholar, from the Research Corporation for Science Advancement, grant ID number 26842. The authors gratefully acknowledge the UW Werk SQuAD (Student Quasar Absorption Diagnosticians), a team of more than 40 dedicated undergraduate researchers since 2017, who made significant contributions to the CGM^2 survey over the last five years and thus enabled some of the science presented in this work. This work benefited from lively Zoom discussions during KITP's "Fundamentals of Gaseous Halos" program, and thus was supported in part by the National Science Foundation under grant No. NSF PHY-1748958.

Software: `astropy` (Astropy Collaboration et al. 2013, 2018, 2022), `linetools` (Prochaska et al. 2017), `matplotlib` (Hunter 2007), `numpy` (Harris et al. 2020), `pandas` (McKinney 2010).

ORCID iDs

Kirill Tchernyshyov https://orcid.org/0000-0003-0789-9939
Jessica K. Werk https://orcid.org/0000-0002-0355-0134
Matthew C. Wilde https://orcid.org/0000-0003-1980-364X
J. Xavier Prochaska https://orcid.org/0000-0002-7738-6875
Todd M. Tripp https://orcid.org/0000-0002-1218-640X
Joseph N. Burchett https://orcid.org/0000-0002-1979-2197
Rongmon Bordoloi https://orcid.org/0000-0002-3120-7173
J. Christopher Howk https://orcid.org/0000-0002-2591-3792
Nicolas Lehner https://orcid.org/0000-0001-9158-0829
John M. O'Meara https://orcid.org/0000-0002-7893-1054
Nicolas Tejos https://orcid.org/0000-0002-1883-4252
Jason Tumlinson https://orcid.org/0000-0002-7982-412X

References

Anand, A., Nelson, D., & Kauffmann, G. 2021, MNRAS, 504, 65
Appleby, S., Davé, R., Sorini, D., Cui, W., & Christiansen, J. 2023, MNRAS, 519, 5514
Aragon Calvo, M. A., Neyrinck, M. C., & Silk, J. 2019, OJAp, 2, 7

Astropy Collaboration, Price-Whelan, A. M., Lim, P. L., et al. 2022, ApJ, 935, 167
Astropy Collaboration, Price-Whelan, A. M., Sipőcz, B. M., et al. 2018, AJ, 156, 123
Astropy Collaboration, Robitaille, T. P., Tollerud, E. J., et al. 2013, A&A, 558, A33
Athanassoula, E., & Beaton, R. L. 2006, MNRAS, 370, 1499
Bahcall, J. N., Jannuzi, B. T., Schneider, D. P., et al. 1991, ApJL, 377, L5
Balogh, M. L., Morris, S. L., Yee, H. K. C., Carlberg, R. G., & Ellingson, E. 1999, ApJ, 527, 54
Barnard, G. A. 1947, Biometrika, 34, 123
Behroozi, P., Wechsler, R. H., Hearin, A. P., & Conroy, C. 2019, MNRAS, 488, 3143
Bender, R., Kormendy, J., Bower, G., et al. 2005, ApJ, 631, 280
Bergeron, J. 1986, A&A, 155, L8
Birnboim, Y., & Dekel, A. 2003, MNRAS, 345, 349
Boettcher, E., Chen, H.-W., Zahedy, F. S., et al. 2021, ApJ, 913, 18
Bordoloi, R., Lilly, S. J., Knobel, C., et al. 2011, ApJ, 743, 10
Bordoloi, R., Wagner, A. Y., Heckman, T. M., & Norman, C. A. 2017, ApJ, 848, 122
Burchett, J. N., Tripp, T. M., Bordoloi, R., et al. 2016, ApJ, 832, 124
Burchett, J. N., Tripp, T. M., Wang, Q. D., et al. 2018, MNRAS, 475, 2067
Cappellari, M. 2017, MNRAS, 466, 798
Carignan, C., Chemin, L., Huchtmeier, W. K., & Lockman, F. J. 2006, ApJL, 641, L109
Catinella, B., Schiminovich, D., Kauffmann, G., et al. 2012, A&A, 544, A65
Chabrier, G. 2003, PASP, 115, 763
Chadayammuri, U., Bogdán, Á., Oppenheimer, B. D., et al. 2022, ApJL, 936, L15
Chen, H.-W., Lanzetta, K. M., & Webb, J. K. 2001, ApJ, 556, 158
Chen, H.-W., Zahedy, F. S., Boettcher, E., et al. 2020, MNRAS, 497, 498
Comparat, J., Truong, N., Merloni, A., et al. 2022, A&A, 666, A156
Cooper, T. J., Rudie, G. C., Chen, H.-W., et al. 2021, MNRAS, 508, 4359
Correa, C. A., Schaye, J., & Trayford, J. W. 2019, MNRAS, 484, 4401
Damle, M., Sparre, M., Richter, P., et al. 2022, MNRAS, 512, 3717
Davé, R., Anglés-Alcázar, D., Narayanan, D., et al. 2019, MNRAS, 486, 2827
Davies, J. J., Crain, R. A., Oppenheimer, B. D., & Schaye, J. 2020, MNRAS, 491, 4462
Davies, J. J., Crain, R. A., & Pontzen, A. 2021, MNRAS, 501, 236
Dekel, A., & Birnboim, Y. 2006, MNRAS, 368, 2
Dorman, C. E., Guhathakurta, P., Seth, A. C., et al. 2015, ApJ, 803, 24
Faerman, Y., Sternberg, A., & McKee, C. F. 2020, ApJ, 893, 82
Falcón-Barroso, J., Sánchez-Blázquez, P., Vazdekis, A., et al. 2011, A&A, 532, A95
Feng, Z.-X., Li, Z., Shen, J., et al. 2022, ApJ, 933, 233
Fielding, D., Quataert, E., McCourt, M., & Thompson, T. A. 2017, MNRAS, 466, 3810
Harris, C. R., Millman, K. J., van der Walt, S. J., et al. 2020, Natur, 585, 357
Heckman, T. M., Norman, C. A., Strickland, D. K., & Sembach, K. R. 2002, ApJ, 577, 691
Ho, S. H., Martin, C. L., & Schaye, J. 2021, ApJ, 923, 137
Hunter, J. D. 2007, CSE, 9, 90
Johnson, S. D., Chen, H.-W., & Mulchaey, J. S. 2015, MNRAS, 449, 3263
Kauffmann, G., Heckman, T. M., White, S. D. M., et al. 2003, MNRAS, 341, 33
Keeney, B. A., Stocke, J. T., Pratt, C. T., et al. 2018, ApJS, 237, 11
Kereš, D., Katz, N., Weinberg, D. H., & Davé, R. 2005, MNRAS, 363, 2
Khoperskov, S., Haywood, M., Di Matteo, P., Lehnert, M. D., & Combes, F. 2018, A&A, 609, A60
Lan, T.-W. 2020, ApJ, 897, 97
Lehner, N., Berek, S. C., Howk, J. C., et al. 2020, ApJ, 900, 9
Lehner, N., Howk, J. C., & Wakker, B. P. 2015, ApJ, 804, 79
Lewis, A. R., Dolphin, A. E., Dalcanton, J. J., et al. 2015, ApJ, 805, 183
Łokas, E. L. 2022, A&A, 667, A27
Martig, M., Bournaud, F., Teyssier, R., & Dekel, A. 2009, ApJ, 707, 250
Masters, K. L., Mosleh, M., Romer, A. K., et al. 2010, MNRAS, 405, 783
Mathews, W. G., & Prochaska, J. X. 2017, ApJL, 846, L24
McKinney, W. 2010, in Proc. 9th Python in Science Conf., ed. S. van der Walt & J. Millman, 56
McQuinn, M., & Werk, J. K. 2018, ApJ, 852, 33
Nelson, D., Kauffmann, G., Pillepich, A., et al. 2018, MNRAS, 477, 450
Newnham, L., Hess, K. M., Masters, K. L., et al. 2020, MNRAS, 492, 4697
Nuza, S. E., Parisi, F., Scannapieco, C., et al. 2014, MNRAS, 441, 2593
Oppenheimer, B. D., Crain, R. A., Schaye, J., et al. 2016, MNRAS, 460, 2157
Oppenheimer, B. D., Davies, J. J., Crain, R. A., et al. 2020, MNRAS, 491, 2939
Park, M., Tacchella, S., Nelson, E. J., et al. 2022, MNRAS, 515, 213
Piotrowska, J. M., Bluck, A. F. L., Maiolino, R., & Peng, Y. 2022, MNRAS, 512, 1052
Planck Collaboration, Ade, P. A. R., Aghanim, N., et al. 2016, A&A, 594, A13
Prochaska, J. X., Tejos, N., Crighton, N., et al. 2017, Linetools/Linetools: Third Minor Release, vv0.3, Zenodo, doi:10.5281/zenodo.1036773
Qu, Z., & Bregman, J. N. 2018, ApJ, 862, 23
Qu, Z., Huang, R., Bregman, J. N., & Li, J.-T. 2021, ApJ, 907, 14
Reines, A. E., & Volonteri, M. 2015, ApJ, 813, 82
Sanchez, N. N., Werk, J. K., Tremmel, M., et al. 2019, ApJ, 882, 8
Sánchez, S. F., Rosales-Ortega, F. F., Iglesias-Páramo, J., et al. 2014, A&A, 563, A49
Schaye, J., Crain, R. A., Bower, R. G., et al. 2015, MNRAS, 446, 521
Stern, J., Faucher-Giguère, C.-A., Hennawi, J. F., et al. 2018, ApJ, 865, 91
Stocke, J. T., Penton, S. V., Danforth, C. W., et al. 2006, ApJ, 641, 217
Suresh, J., Rubin, K. H. R., Kannan, R., et al. 2017, MNRAS, 465, 2966
Tchernyshyov, K., Werk, J. K., Wilde, M. C., et al. 2022, ApJ, 927, 147
Tejos, N., Prochaska, J. X., Crighton, N. H. M., et al. 2016, MNRAS, 455, 2662
Terrazas, B. A., Bell, E. F., Pillepich, A., et al. 2020, MNRAS, 493, 1888
Tillman, M. T., Burkhart, B., Tonnesen, S., et al. 2023, ApJL, 945, L17
Tripp, T. M., Sembach, K. R., Bowen, D. V., et al. 2008, ApJS, 177, 39
Tubbs, A. D. 1982, ApJ, 255, 458
Tumlinson, J., Thom, C., Werk, J. K., et al. 2011, Sci, 334, 948
Voit, G. M. 2019, ApJ, 880, 139
Weinberger, R., Springel, V., Hernquist, L., et al. 2017, MNRAS, 465, 3291
Werk, J. K., Prochaska, J. X., Thom, C., et al. 2013, ApJS, 204, 17
White, S. D. M., & Rees, M. J. 1978, MNRAS, 183, 341
Wilde, M. C., Werk, J. K., Burchett, J. N., et al. 2021, ApJ, 912, 9
Williams, B. F., Dolphin, A. E., Dalcanton, J. J., et al. 2017, ApJ, 846, 145
Winkel, N., Pasquali, A., Kraljic, K., et al. 2021, MNRAS, 505, 4920
Zahedy, F. S., Chen, H.-W., Cooper, T. M., et al. 2021, MNRAS, 506, 877
Zahedy, F. S., Chen, H.-W., Johnson, S. D., et al. 2019, MNRAS, 484, 2257
Zinger, E., Pillepich, A., Nelson, D., et al. 2020, MNRAS, 499, 768